The influence of remote aerosol forcing from industrialised economies on the future evolution of East and West African rainfall

The Influence of Remote Aerosol Forcing from Industrialized Economies on the Future Evolution of East and West African Rainfall

CLAIRE SCANNELL,[a] BEN B. B. BOOTH,[a] NICK J. DUNSTONE,[a] DAVID P. ROWELL,[a] DAN J. BERNIE,[a] MATTHEW KASOAR,[b,c] APOSTOLOS VOULGARAKIS,[b] LAURA J. WILCOX,[d,e] JUAN C. ACOSTA NAVARRO,[f,g,h] ØYVIND SELAND,[i] AND DAVID J. PAYNTER[j]

[a] *Met Office Hadley Centre, Exeter, United Kingdom*
[b] *Department of Physics, Imperial College London, London, United Kingdom*
[c] *Grantham Institute-Climate Change and the Environment, Imperial College London, London, United Kingdom*
[d] *National Centre for Atmospheric Science, Leeds, United Kingdom*
[e] *Department of Meteorology, University of Reading, Reading, United Kingdom*
[f] *Department of Environmental Science and Analytical Chemistry, Stockholm University, Stockholm, Sweden*
[g] *Bolin Centre for Climate Research, Stockholm University, Stockholm, Sweden*
[h] *Earth Sciences Department, Barcelona Supercomputing Center, Barcelona, Spain*
[i] *Norwegian Meteorological Institute, Oslo, Norway*
[j] *NOAA/Geophysical Fluid Dynamics Laboratory, Princeton, New Jersey*

(Manuscript received 25 October 2018, in final form 16 August 2019)

ABSTRACT

Past changes in global industrial aerosol emissions have played a significant role in historical shifts in African rainfall, and yet assessment of the impact on African rainfall of near-term (10–40 yr) potential aerosol emission pathways remains largely unexplored. While existing literature links future aerosol declines to a northward shift of Sahel rainfall, existing climate projections rely on RCP scenarios that do not explore the range of air quality drivers. Here we present projections from two emission scenarios that better envelop the range of potential aerosol emissions. More aggressive emission cuts result in northward shifts of the tropical rainbands whose signal can emerge from expected internal variability on short, 10–20-yr time horizons. We also show for the first time that this northward shift also impacts East Africa, with evidence of delays to both onset and withdrawal of the short rains. However, comparisons of rainfall impacts across models suggest that only certain aspects of both the West and East African model responses may be robust, given model uncertainties. This work motivates the need for wider exploration of air quality scenarios in the climate science community to assess the robustness of these projected changes and to provide evidence to underpin climate adaptation in Africa. In particular, revised estimates of emission impacts of legislated measures every 5–10 years would have a value in providing near-term climate adaptation information for African stakeholders.

1. Introduction

Sub-Saharan and East Africa have experienced both prolonged periods of drought and increased flooding over the last 50 years (Dai et al. 2004; Held et al. 2005; Dai 2012; Nicholson 2016, 2017), with devastating consequences on society. There is substantial concern that climate change and population increases will only exacerbate vulnerabilities of these developing nations. Analysis of the risks of future change have, to date, primarily focused on the context of the steady past and future rise in greenhouse gas (GHG) emissions, the impacts of which will be substantial (e.g., IPCC 2014a,b; Chadwick 2016) but, nevertheless, lag significantly behind emission rates due to their long atmospheric lifetimes.

In the African context, much of the current requirement for future climate change projection information focuses on near-term, 10–40-yr time-scale climate adaptation. On

Denotes content that is immediately available upon publication as open access.

Corresponding authors: Ben B. B. Booth, ben.booth@metoffice.gov.uk; Claire Scannell, claire.scannell@metoffice.gov.uk

DOI: 10.1175/JCLI-D-18-0716.1

this time scale, different GHG emission pathways (such as those used in CMIP5) drive only a relatively small spread in global warming due to the long atmospheric lifetimes of the gases involved (Hawkins and Sutton 2009). In contrast, changes in other industrial pollutants such as aerosols show a strong potential to drive diversity in near-term changes in atmospheric composition. The much shorter atmospheric lifetime of aerosols, numbered in days, means that differences in these pathways have the potential to play a much more rapid role in driving the spread of near-term climate changes. Yet, we currently lack a range of standard multimember climate model experiments explicitly designed to explore these potential near-term pathways.

Scenarios of potential near-term aerosol emissions are particularly pertinent for African climate, as aerosol emissions from remote industrialized economies have been implicated in driving historical changes in the region. The northward and southward extent of the seasonal rainfall across the tropics globally has been linked to changes in anthropogenic aerosols in the Northern Hemisphere (Shindell et al. 2012; Hwang et al. 2013) via a well-established mechanism. The Northern Hemispheric aerosol predominance arises from the comparatively short atmospheric lifetimes (numbered in days) that keep concentrations close to the sources of the aerosol precursor emissions in the industrialized economies. This leads to a stronger net surface cooling in the Northern Hemisphere relative to the Southern Hemisphere (Myhre et al. 2013), establishing a hemispheric asymmetry in temperature where the Southern Hemisphere has warmed faster than the Northern Hemisphere (Shawki et al. 2018; Wilcox et al. 2013). This warming asymmetry led to a cross-equatorial transfer of energy across the tropics and a southward shift of the rainbands (Rotstayn and Lohmann 2002; Chang et al. 2011; Bollasina et al. 2011; Allen et al. 2015).

In West Africa, this same tropics wide mechanism is thought to have driven an important part of the observed decline in the 1970s and 1980s in the Sahelian summer rainfall (Kawase et al. 2010; Ackerley et al. 2011; Chang et al. 2011; Booth et al. 2012; Dong et al. 2014; Allen et al. 2015; Dong and Sutton 2015). This decline is linked to slower warming in the North Atlantic between the 1960s and 1980, compared to the South Atlantic (Hoerling et al. 2006; Wilcox et al. 2013) due to larger North Atlantic cooling due to increasing aerosol concentrations during that time (Booth et al. 2012). This North Atlantic cooling, in turn, is linked to increases in aerosol precursors from both North America and Europe (Undorf et al. 2018).

Similar links have not clearly been made with East African historical changes. While seasonal migrations of the tropical monsoon system can be expected to also impact East African rains, the relationship between these shifts and the East African monsoon is less clear. Interactions with large topographical gradients (such as the Ethiopian Highlands) and the East African jet result in complex seasonal monsoon migration of the rains that does not conform to the more north–south-like migrations seen in West Africa. Past anthropogenic aerosol changes have been potentially linked to the East African paradox (Rowell et al. 2015). This refers to the observed decline in the East African long rains (March, April, May season), one of the two main East African rainfall seasons. This decline is unprecedented in the observed record (Viste et al. 2013; Liebmann et al. 2014; Rowell et al. 2015; Nicholson 2017) and contrasts with simulations that suggest that GHG impacts are likely to enhance rainfall during the long rains (hence the paradox). Existing literature links the long rains to regional SST variations in the Indian Ocean (Nicholson 2016). Simulations forced by historical aerosol changes do not capture the long rains decline, but many of them do project on to the Indian and Pacific SSTs that are thought to be linked to these changes (Rowell et al. 2015) and, as such, it remains one of the few hypotheses that have yet to be ruled out. Historical drivers of changes in the East African short rains (September–December rains) have received less attention in the published literature with most focus on shorter, seasonal-time-scale drivers (e.g., Nicholson 2015). In part this is because the short rains have not experienced as marked decadal and longer time-scale variations as those experienced in the recent long rains decline.

Anthropogenic aerosols arise as a by-product of fossil fuel usage, cooking fires, and land-use practices. In terms of their global radiative forcing impact, sulfate aerosols, which form from SO_2 emissions from burning fossil fuels, are the dominant anthropogenic component (Myhre et al. 2013). For the purpose of this analysis we focus on sulfate aerosols in particular, as they have also been shown to be most important for global tropical precipitation shifts generally (Allen et al. 2015) and Sahel shifts specifically (Westervelt et al. 2018). For much of the early part of the last century, SO_2 emissions, the precursor of sulfate aerosols, increased in line with increased GHG emissions. Links between sulfate aerosols and air quality and acid rain led to sequential implementation of clean air legislation in Europe and North America. These measures led to aerosol declines in these regions from the 1980s onward (Manktelow et al. 2007). Changing fuel mix and technological approaches (such as implementation of chimney scrubbers) have enabled these legislative requirements to be met. Aerosol emission increases in developing economies continued through the second half of the last century, particularly in the rapidly industrializing Asian economies. However, similar air quality drivers have led to a recent stabilization and a

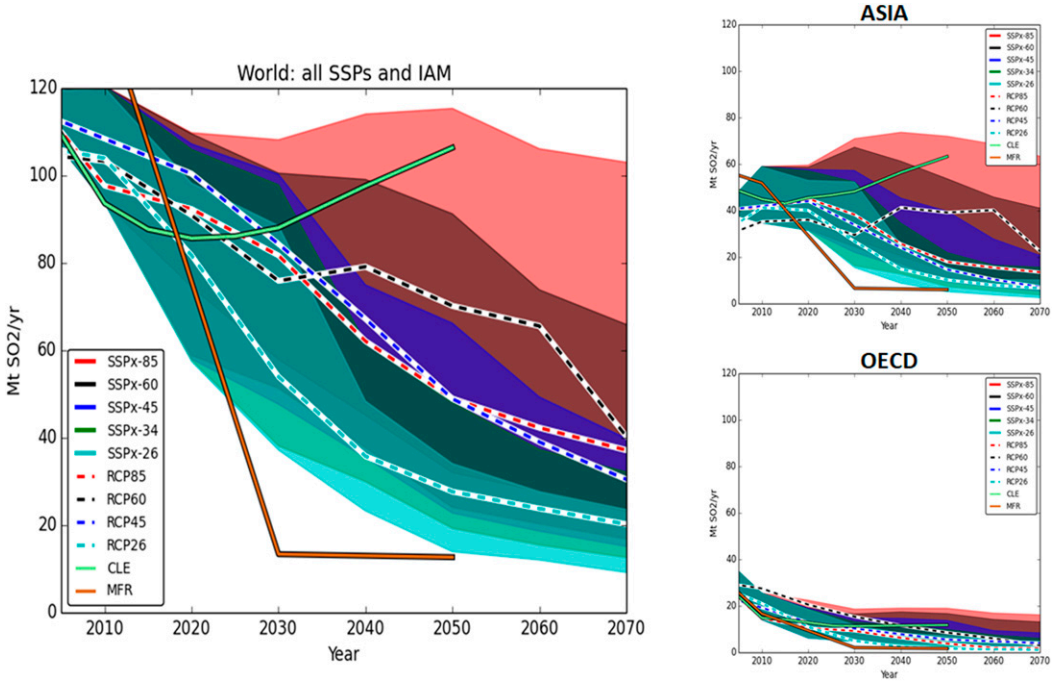

FIG. 1. (left) Global spread of SO_2 emissions for all shared socioeconomic pathway (SSP) scenarios and integrated assessment models (IAMs) (colored bands represent different RF ranges). The dashed lines represent RCP2.6, RCP4.5, RCP6.0, and RCP8.5 from the existing CMIP5 experiments. The solid light green line (CLE) and orange line (MTFR) represent SO_2 emissions for current day legalization and maximum feasible reductions, respectively, for RCP GHG concentrations. (top right) Asian and (bottom right) OECD spread of SO_2 emissions for all SSPs and IAMs.

decrease of SO_2 emissions from China (Lu et al. 2011; Zheng et al. 2018).

Given the existing links between aerosol emissions and past changes in African rainfall, it is important to understand the potential African impact of future anthropogenic aerosol changes. Figure 1 shows the range of future SO_2 emissions sampled within the shared socioeconomic pathways (SSPs) outlined in Riahi et al. (2017). These project a broad range of potential emission pathways, ranging from little global change from present day to large reductions, approaching 90% reductions in the short 40-yr time horizon relevant for African climate projections (representing an emission uncertainty of almost 100 Mt $SO_2\,yr^{-1}$ by 2050). However, existing CMIP5 generation climate model projections do not explore this wider range of potential aerosol scenarios. Reflective of their remit to explore end-of-century climate changes, they all follow very similar assumptions that air quality measures will be adopted universally and aggressively (Van Vuuren et al. 2011). These CMIP5 simulations, and a number of more idealized aerosol emission removal experiments, do provide useful indications of the potential impact on West African rainfall. Under scenarios of future aerosol decreases (as represented in CMIP5's RCP scenarios), these changes act to shift tropical precipitation northward in response to more rapid warming in the Northern Hemisphere, via similar mechanisms to those outlined above for historical changes (Rotstayn et al. 2015; Allen 2015). Similarly, idealized experiments designed to explore the impact of removal of North American SO_2 emissions (Westervelt et al. 2017) or removal of a wider set of regional aerosol precursor emissions, including from North America and Europe (Westervelt et al. 2018), show that removal of these aerosols leads to a northward ITCZ shift and moistening over the Sahel via a similar mechanism. What we do not currently have are climate-model-based climate projections that span the range of near-term aerosol changes. Such experiments would be needed to inform the time scale and emergence of rainfall impacts that could result from different near-term aerosol emission pathways.

Unlike for West Africa, there is no existing literature exploring the impact of future aerosol changes on East African rains, either from preexisting CMIP5-era simulations or idealized experiments. The East African rainfall impacts from future aerosol emission pathways presented here is new.

Here we set out to assess the potential impact of future aerosol reductions (or lack of) on African rainfall, focusing on East and West Africa as two particularly vulnerable and climatically distinct regions:

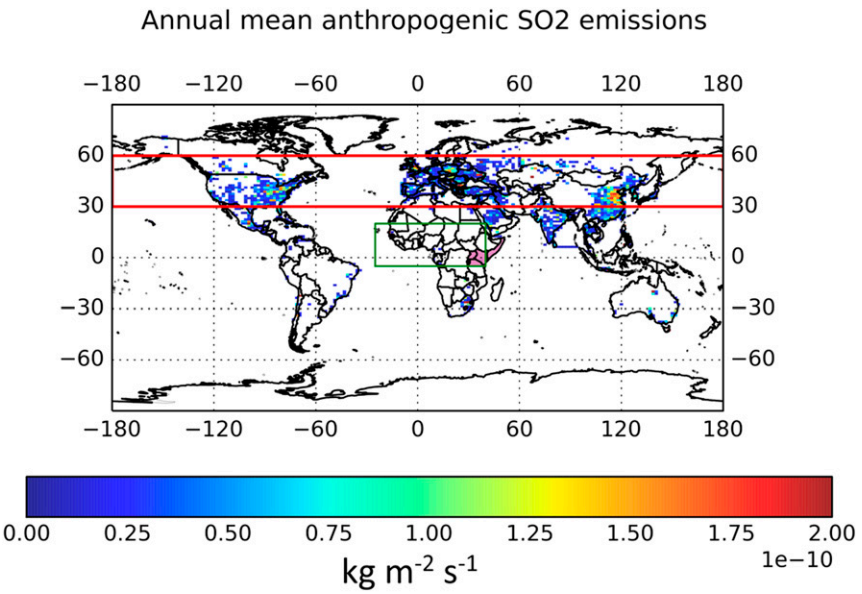

FIG. 2. The anthropogenic SO_2 ACCMIP emissions based on the year 2000. The red box represents the NHML region where SO_2 emissions are removed in the idealized experiment. The shaded pink region in Africa represents the East African domain used in subsequent Hovmöller plots. The green box indicates the dimension of maps in Figs. 7 and 9 that explore Sahel rainfall impacts in West Africa.

In section 2, we make use of an idealized experiment exploring the removal of anthropogenic SO_2 from the Northern Hemisphere midlatitudes to explore the details of how these changes would impact the monsoon systems in one particular model, HadGEM3-ES. Here we refer to SO_2 emissions from the industrialized economies as industrial or anthropogenic aerosol emissions (interchangeably). These simulations are similar to earlier idealized regional emission removal experiments (Westervelt et al. 2017, 2018) but span the Northern Hemisphere extratropics. The multicentury length of these simulations provides clear signal to noise that can help identifying the regions and seasons that we would expect to be most sensitive to differences in future aerosol emission scenarios. Where the responses in the idealized simulations are similar to the scenario experiments described in section 3 (where changes in the wider range of aerosol are also simulated) this may point to the relative importance of SO_2 emissions in driving these changes.

In section 3, we discuss these changes within the context of the wider emission scenario uncertainty, Fig. 1. We use bespoke emission scenarios from the Evaluating the Climate and Air Quality Impacts of Short-Lived Pollutants (ECLIPSE) experiments (Stohl et al. 2015) to explore the potential future uncertainty in emission scenarios. In particular, we focus on the time evolution of any climate changes and compare these to internal variability in the near 10–40-yr time horizon. The ECLIPSE scenarios explore a much wider spread of emission uncertainty than earlier CMIP5 simulations, ranging from little change in 2050 from present-day emissions, to rapid reductions that realize most of the cuts simulated in the idealized experiments in section 2. We make use of transient simulations with three climate models (HadGEM3-GC2, GFDL CM3, and NorESM1-M) driven by scenarios designed to envelope this range of future aerosol emission changes [maximum technological feasible reduction (MTFR) and current legalization (CLE); Fig. 1]. Each climate model provides 3–4 ensemble members that enable us to illustrate the time scales and spatial locations where we would expect the climate impact to emerge from natural rainfall variability. These transient climate change experiments provide an opportunity to assess the time scale of emergence and to assess where these changes are robust across the different climate models.

2. Regional response to anomalous aerosol emissions

Here we examine the regional response to pan-hemispheric reductions in SO_2 emissions, the main precursor to sulfate aerosols. In the following experiments, the SO_2 emissions are abruptly decreased to zero across the Northern Hemisphere midlatitude (NHML) region (red box in Fig. 2). All other emissions are held at year 2000

levels in both the control experiments and the perturbed experiment, to explicitly look at the regional response to a complete removal of industrial SO_2 emissions.

a. Experimental setup

The Hadley Centre Global Environmental Model 3–Earth System (HadGEM3-ES) model (Hardiman et al. 2017) is the fully coupled configuration with Global Atmosphere 4.0 (HadGEM3-GA4; Walters et al. 2014) that was used to run the idealized model experiment. This experiment was coupled ocean–atmosphere using the Coupled Large-Scale Aerosol Simulator for Studies in Climate (CLASSIC) aerosol scheme (Martin et al. 2006, 2011; Bellouin et al. 2011). To quantify the impact of unforced variability, six control experiments were also run with full, global, perpetual year 2000 conditions, including Atmospheric Chemistry and Climate Model Intercomparison Project (ACCMIP) aerosol emissions. Each control run had a different atmospheric initial state but the same ocean initial state.

The idealized experiment was branched from a single control experiment where the SO_2 emissions were switched to zero in the northern midlatitude region (corresponding to the red box in Fig. 2) at the beginning of the simulation. Perpetual year 2000 conditions were otherwise retained, including ACCMIP SO_2 emissions outside this midlatitude region. This experiment was spun up for 100 years and run for a further 200 years. The long integrations enabled an exploration of the signals in response to this reduction and to step back from questions about the time scales that these emerge. The analysis shown here is for the last 150 years after the climate has equilibrated to any changes (from both control and perturbed experiments). For full details on experimental setup, aerosol schemes, and model references, see Shawki et al. (2018) and Kasoar et al. (2018, 2016).

b. Influence of large-scale drivers on African rainfall

As noted in the introduction the northward/southward extent of the tropical rainbands are influenced by both large- and local-scale drivers. The presence of anthropogenic SO_2 aerosols across the Northern Hemisphere midlatitudes preferentially cools the Northern Hemisphere (Shawki et al. 2018). Removing these aerosols in HadGEM3-GA4 results in a global impact on temperature of 0.821 ± 0.052 K, largely constrained to the Northern Hemisphere (Fig. 3). Removing industrial/anthropogenic SO_2 emissions across the Northern Hemisphere midlatitudes resulted in a globally warmer world, with stronger hemispheric warming for the Northern Hemisphere (1.18 ± 0.08 K) compared to the Southern Hemisphere (0.467 ± 0.044 K) for the 150-yr average signal from the year 2000 conditions (Fig. 3).

Figure 4 illustrates the climatological rainfall ($2\,\text{mm day}^{-1}$ contour) in each season from the control simulations, and the impact on these rainfall patterns from removing industrial SO_2 aerosols from the Northern Hemisphere (colored shading). The climatological rainfall shifts toward the warmer hemisphere between boreal and austral summers—with the maximum northward extent occurring during June, July, and August and the most southward extent in December, January, and February. Removal of industrial aerosols from the Northern Hemisphere leads to a northward shift in the seasonal rains (colored shading), due to the stronger warming in the Northern Hemisphere midlatitudes relative to the Southern Hemisphere (Fig. 3). This is in line with earlier work that linked declining aerosol emissions with a northward shift of the tropical monsoon system via preferential warming of the Northern Hemisphere (Allen 2015; Rotstayn et al. 2015; Westervelt et al. 2017, 2018). The boreal summer (JJA) is climatologically important as it is the only season during which rainfall reaches the Sahel region across West and central Africa (roughly 10°–20°N). During this season, the northern shoulder of this rainfall band extends farther northward due to the enhancement of the hemispheric heating contrast. However, there is a notable increase in precipitation on the northern shoulder of the tropical rainfall band for all seasons. In the austral summer, when warmer Southern Hemispheric temperatures lead to seasonal rains in their most southern extent, we also see a northward shift of rainfall due to aerosol reductions. Here the Northern Hemispheric warming (Fig. 3) weakens the temperature gradient across the equator, limiting the seasonal southward shift.

For much of East Africa, both boreal and austral summers coincide climatologically with drier conditions and the main rainy seasons occur during the monsoon transition seasons, within the long rains (March, April, and May) and short rains [September, October, November, and December (SOND)]. Here too, in Fig. 4 we see a general northward displacement consistent with the Northern Hemispheric warming, although this impact is stronger, more coherent and statistically significant in the short rains season (SOND). In the long rains (MAM) there are no statistically significant changes (Fig. 4). The reason for this more coherent shift in SOND is likely to be linked to the enhancement of the strong local north–south gradient evident in this season (Fig. 3). The Saharan heat low (which extends over the Arabian Peninsula) builds up over JJA and extends into SOND, warming faster than the equator, driving a locally enhanced north–south temperature gradient in the East African region. March–May conditions see much weaker north–south gradient changes (Fig. 3) and this

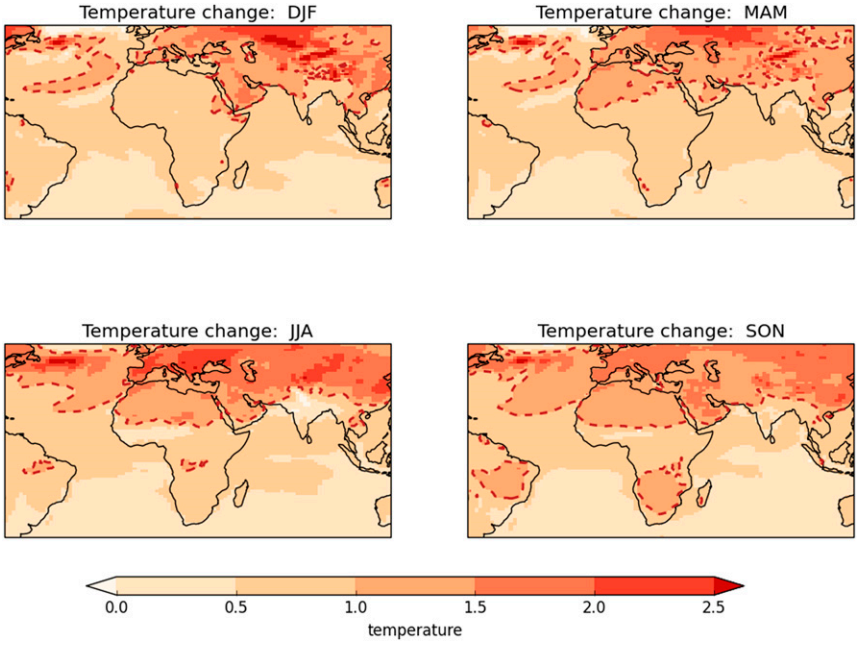

FIG. 3. The 150-yr seasonal temperature change between the control experiments set at year 2000 conditions and the idealized experiments with zero SO_2 emissions over the NHML domain. The dashed line highlights the 1-K increase contour, emphasizing the larger north–south gradients that are established in JJA and SON over the Saharan heat low and enhanced gradients driven by strengthening of the Arabian heat low in JJA, SON, and DJF.

may be why the rainfall response is both weaker and less coherent and not statistically significant (except over the Indian Ocean).

c. *Impact of abrupt removal of NHML anthropogenic aerosols on East Africa*

East Africa experiences most of its rain as the monsoon systems transition northward and southward between boreal and austral summers. Figure 5 shows a Hovmöller plot of this transition for the East African region indicated in Fig. 2. The climatological northward progression through the long rains is captured, as is the southward progression through the short rains. It should be noted, though, that while the HadGEM3 model captures the timing and position of the bimodal rainfall distribution in the region, in common with other models (Yang et al. 2015) it tends to underestimate the intensity of the long rains and overestimate the intensity of the short rains (Fig. 5). This is a result of model bias that ultimately causes a warm SST bias in OND because of insufficient ocean dynamical cooling and latent flux, while insufficient shortwave radiation and excess latent heat flux mainly contribute to the cool SST bias in MAM (Yang et al. 2015). Yang et al. (2015) focused on OND, but we expect their findings to hold for the longer SOND season considered here. Because of this climatological bias, we examine relative changes from the model to understand how the precipitation responds (which we would expect to be less sensitive to the bias compared to absolute changes).

Figure 5 shows the annual precipitation response over the East African domain to the removal in industrial SO_2 aerosols from the NHML region, averaged over 150 years. A clear and substantial (stippling in the bottom panel of Fig. 5) signal over the East African region is observed in the HadGEM3 simulations for the short rains. At the beginning of the season, there is a clear reduction in rainfall across the entire domain, with some locations seeing a reduction of as much as 50% at the beginning of October during traditionally heavy rain periods. This is followed by a sustained period of intensification of rainfall of up to 40% and extension of the OND season into January and February. This suggests a delayed propagation southward of the tropical rainbands and, as a result, a delay in onset to the short rains. This precipitation response is particularly impactful for the region. For example, Southern Hemisphere latitudes (southern Kenya, Great Lakes, and northern Tanzania) could see increases of up to 20% during an already significantly wet period in January, while Northern Hemisphere latitudes (Somalia) could see increases of up 40% toward the end of October when a large fraction

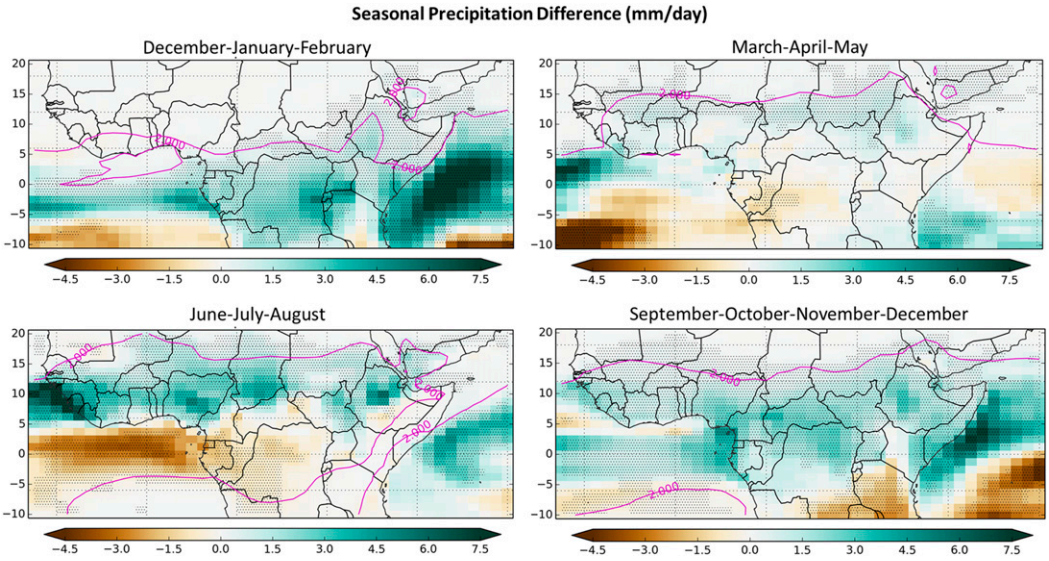

FIG. 4. The 150-yr seasonal average rainfall absolute difference between the climatology (average of the control experiments) and the idealized NHML experiment (anthropogenic SO_2 reduced to zero over the NHML domain). The pink contour indicates the mean position of the 2 mm day^{-1} rainfall contour, as an indicator of the extent of tropical rainfall within each season. The stippling denotes where the rainfall difference is significant at the 10% level relative to the 150-yr rainfall variability across the six control simulations.

of this region's precipitation currently occurs and a greater than 40% increase in December and January during traditionally drier periods.

Interestingly, Dunning et al. (2018) see a similar delay in the onset of the short rains in CMIP5 climate projections, which they attribute to greater warming (relative to surrounding regions) of the Saharan heat low (see Fig. 5 in Dunning et al. 2018). A very similar pattern of warming is seen in Fig. 3, suggesting an enhanced desert warming and delay in the short rains seen also in CMIP5, which may well be due to the aerosol reductions in the CMIP5 scenarios.

For the long rains season, MAM, the precipitation response is much less sizeable (compared to the short rains) with very few points meeting the $\pm 1\sigma$ criteria (values outside $\pm 1\sigma$ of the controls) (stippling in Fig. 5), and no points meeting the $\pm 2\sigma$ criteria (stippling in Fig. 6). Due to the lack of statistical significance of any changes, we do not explore the impact of idealized SO_2 reductions on the future long rains any further.

Figure 6 illustrates the spatial complexity of the precipitation response to the removal of SO_2 emissions in the NHML region for the short rains. The Hovmöller plot (Fig. 6, bottom) clearly illustrates the strong and substantial (values outside $\pm 2\sigma$ of the controls—stippling) latitudinal rainfall response. The spatial plots (Fig. 6, middle), however, illustrate a more complex picture of the rainfall distribution throughout the season. These indicate a weaker longitudinal transition alongside the latitudinal transition, where enhanced rainfall switches from coastal Kenya to the more central lakes region in December. This suggests that the enhanced rainfall simulated in the model toward the end of the short rains of up to 20% is concentrated inland rather than at the coast and could have a large impact on the central lakes regions.

d. Impact of abrupt removal of NHML anthropogenic aerosols on West Africa

The HadGEM3-ES model simulates well the observed climatological rainfall over the Sahel, including the western coastal, Cameroonian, and Ethiopian maxima (Fig. 7). The model shows some indications that the climatological maximum on the southwest coast is located farther south than observed; however, the latitudinal location and intensity of the central and eastern locations are well reproduced. We discussed earlier the impact of removal of industrial sulfate aerosols from the Northern Hemisphere on the temperature pattern. The enhanced warming north of the Sahel (Saharan heat low; see Fig. 3) drives a northward shift of the monsoon rainband. The rainfall impact on the northern shoulder is the more substantial change. These changes range between 0.5 and 1.0 mm day^{-1} increases over Nigeria and southern Chad (central Sahel), Ethiopia (eastern Sahel), and inland Guinea and Ivory Coast (western Sahel). The changes exceed 1.5 mm day^{-1} increases along the western Sahel seaboard (such as coastal

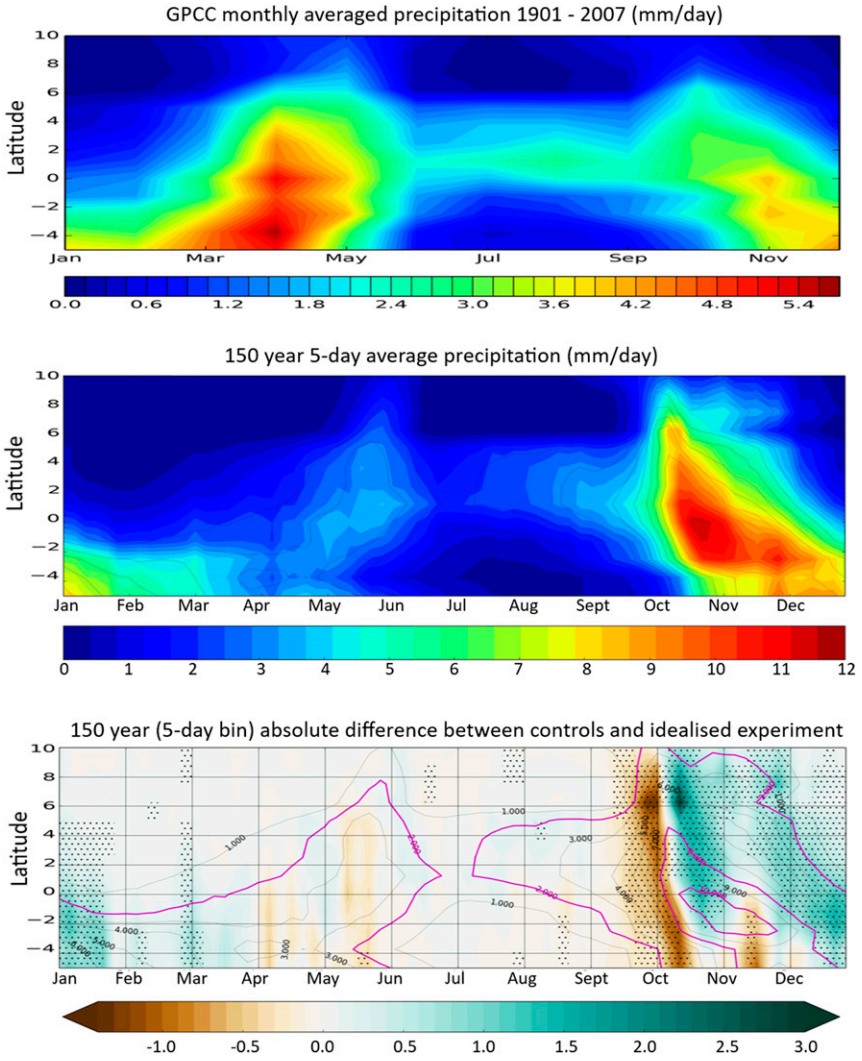

FIG. 5. (top) GPCC observations Hovmöller plot for monthly averaged precipitation 5-day bins across the whole time series (1901–2007) over the East African domain (see Fig. 2) from January to December. (middle) Hovmöller plot of 150-yr, 5-day bins, average climatological precipitation (mm day^{-1}) over the East African domain from the ensemble average of the control 2000 experiments. The East African domain (and NHML region) can be seen in Fig. 2. (bottom) Absolute difference between the control ensemble average precipitation and idealized experiment for SO_2 emissions set to zero over the NHML region. The 2 mm day^{-1} control climatology contour line (based on the middle panel) is highlighted. Here the stippling represents values that exceed $\pm 1\sigma$ of the six control experiments.

Senegal, Guinea, and Liberia). The percentage change (Fig. 7, lower right) provides an indication over which regions these changes represent a large fraction of present-day rainfall. These changes can represent an increase of up to 25% in northern Nigeria and southern Chad and increases centered on the Senegalese coastal region.

This picture of aerosol reductions leading to Sahel moistening is consistent with existing studies that link historical increases in Northern Hemispheric aerosols with cooler temperatures over the Atlantic and the wider extratropics (Hoerling et al. 2006; Kawase et al. 2010; Ackerley et al. 2011; Booth et al. 2012). These impacts on north–south temperature gradients are in turn linked to the historic drying over the Sahel region. The pattern of observed rainfall declines in the 1970s and 1980s showed the largest impacts in three main regions of west, central, and eastern Sahel. These regions match those showing the largest magnitude increases in Fig. 7 (lower left). The response to these idealized

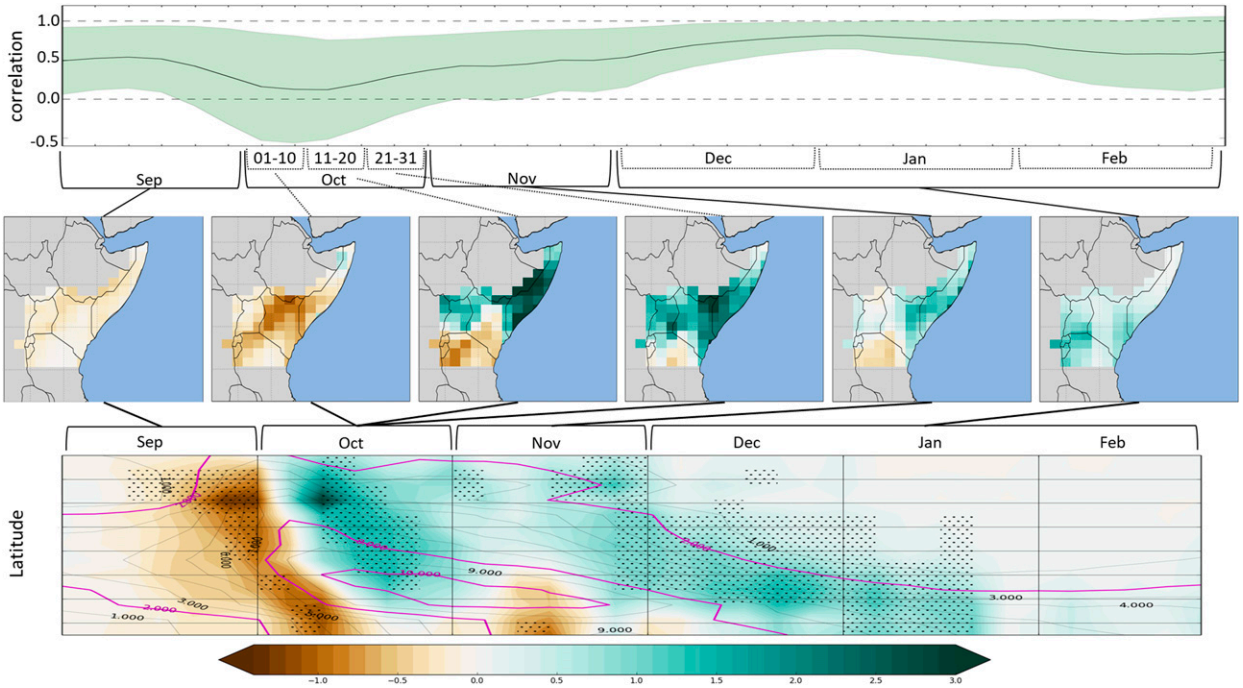

FIG. 6. (top) The spatial anomaly correlation between consecutive 5-day bins indicating when the pattern of the precipitation response changes. (middle) The spatial progression of the precipitation response throughout the season for the East African domain with this lengthening during periods of slower evolution. The time periods of each are indicated by the gray lines pointing to the relevant periods in the top and bottom panels. (bottom) The 150-yr 5-day average precipitation response (absolute difference) to a switch off of anthropogenic SO_2 emissions in the NHML region centering on the OND rain season. The stippling represents a substantial signal outside of $\pm 2\sigma$ from the ensemble mean of the control experiment. The climatological rainfall contours (pink contour lines) are also shown to help reference where the change occurs with respect to the climatological onset and withdrawal. The units for rainfall change and climatology are in mm day^{-1}.

experiments, together with the existing literature, points to a coherent picture of how the Sahel responded and is likely to respond to increases (historical) and projected future SO_2 declines.

3. Projected range of future impacts

a. Impact on Africa of global aerosol emission uncertainties

The idealized experiments give a clear picture of the spatial and temporal patterns of potential future changes in African precipitation, in response to a complete reduction in remote SO_2 emissions. Over West Africa, the patterns are consistent with existing idealized simulations carried out with other climate models (Westervelt et al. 2018). However, a key question for decision-makers is, How much of this precipitation response could be realized under plausible transient scenarios? The forthcoming SSP emission scenarios (O'Neill et al. 2016; Riahi et al. 2017) provide a context to explore these changes. Riahi et al. (2017) show how future aerosol emissions (Fig. 1) respond to a broad range of drivers including fossil fuel emissions (socioeconomic, degrees of climate mitigation), with some sampling of different air quality drivers (which are linked to how clean the energy production would be). At one end of this wider SSP aerosol emission range we could see reductions approaching 90% of present-day emissions by 2050. At this end of the range, scenarios represent strong mitigation, achieving the global commitment to a "well below 2°C" world, in line with the Paris Agreement. Here the reduction of aerosol emissions is associated with the rapid decarbonization required to meet these targets. At the other end of this spectrum, in fossil fuel dominated business as usual shared socioeconomic pathways, we could expect to see scenarios with very little change in global emissions with respect to present-day emissions. The response of the idealized runs is therefore a useful indication of the magnitude of the climate impact, and temporal/spatial locations, that we would expect to arise from the SSP scenario range.

These differences are important to highlight as they have implications for how we view changes in current CMIP5 climate projections. CMIP5 scenarios all assume some aerosol emission cuts (Fig. 1) and as such would be

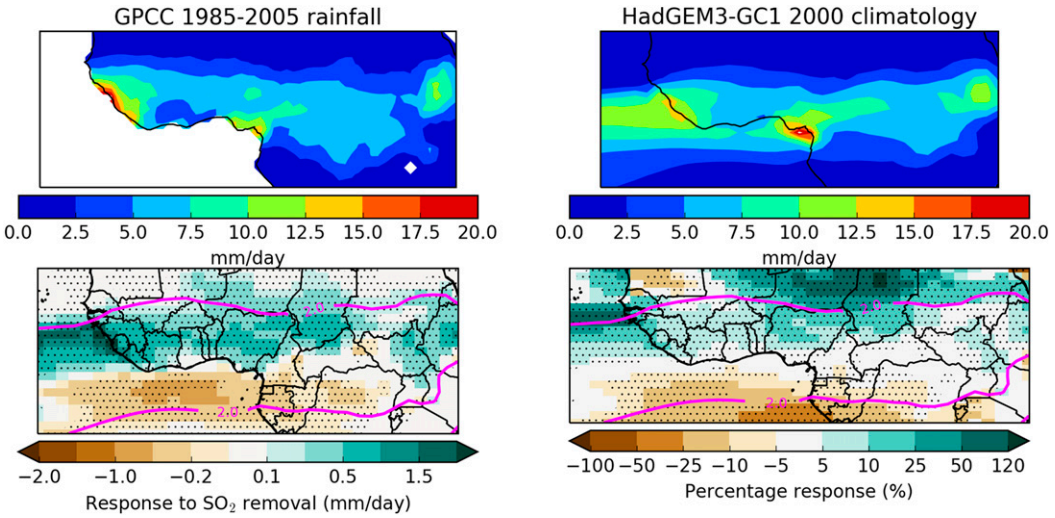

FIG. 7. West African JJA (June–August) rainfall (mm day^{-1}) in the (top left) GPCC climatology estimate, 1985–2005, (top right) the climatological rainfall in the model, (bottom left) the change (mm day^{-1}) arising from removal of Northern Hemispheric aerosol emissions, and (bottom right) the percentage change. Rainfall changes significant at the 10% level with respect to the control variability are indicated by stippling. The purple contour (bottom panels) denotes the 2 mm day^{-1} threshold in the 2000 climatology to highlight where the changes occur with respect to the current tropical rainbands. The increases on the northern shoulder and the decrease south of the JJA rain belt are consistent with a general northward shift in the tropical rainband location. The rainfall increase changes occur on the northern shoulder of the present-day tropical rainbands, with the largest changes coinciding with the location of larger present-day rainfall (western, central, and eastern Sahel). These changes represent a larger percentage of present-day rainfall (lower right) where they occur on the northern shoulder of the present-day monsoon in the central Sahel region (northern Nigeria, Niger, and Chad) and the Senegalese coastal region

expected to capture some of the rainfall impacts in East and West Africa linked to these cuts [such as the projected delay in monsoon onset in Dong et al. (2014)]. The wider scenario context, however, suggests that these changes may be more pronounced than anything found in the CMIP5 archive under stronger industrial aerosol reductions, or may in fact lead to much reduced changes should aerosol reductions not materialize.

New simulations in the forthcoming CMIP6 effort could potentially better represent the future emission range. How effective CMIP6 modeling does so, however, will depend on how the Scenario Model Intercomparison Project (ScenarioMIP; O'Neill et al. 2016) subsamples the wider matrix of SSP, radiative forcing (RF) targets, and the contributing integrated assessment models that produced the emission datasets shown in (Amann et al. 2013) (Fig. 1). The core Tier 1 CMIP6 experiments suggested under ScenarioMIP sample the diagonal between sustainability (SSP1)–low RF targets out to continued fossil fueled development (SSP5)–high RF targets. Therefore, we anticipate that there may still be a need for other scenarios that target near-term (10–40 yr) air quality drivers before climate modeling will be in a position to inform African climate impacts from aerosol emissions. We cover the climate response to two such scenarios in the next subsection.

b. *Precipitation response within explicit air quality–driven climate change scenarios*

The ECLIPSE project explicitly set out to explore the aerosol emission changes and subsequent climate impact associated with air quality measures, and we make use of climate models driven by two ECLIPSE scenarios here. These ECLIPSE scenarios (CLE and MTFR) take a single socioeconomic pathway (CMIP5's RCP4.5) and explore what industrial aerosol emissions could look like should air quality measures not advance over present measures (CLE) or exploit all currently available technologies to reduce emissions (MTFR). The CLE scenario assumes that all existing and planned legislation on emissions is fully implemented, perfectly enforced, and delivers the expected emission reductions. In this scenario East Asian emissions, driven by China, increase until 2020 before any decline, while South Asian emissions, driven by India, continue to increase (Stohl et al. 2015). The MTFR scenario assumes that all currently available emission reduction technologies are unconditionally implemented but no nontechnical measures are accounted for, such as behavioral changes.

All nations begin to reduce their emissions gradually in 2015, with full implementation by 2030 (Stohl et al. 2015). These differences are smaller in Europe and North America, where three decades of air quality legislation have already addressed many of the easier technological options. They are greater over Asia where the larger present-day emissions and the greater range of technological options lead to the potential for larger aerosol emission reductions (see Fig. 1). They also sample a much wider range of the future uncertainty in aerosol emissions than CMIP5 RCPs. As illustrated in Fig. 1, by 2050, the CLE and MTFR scenarios capture a wider initial spread of aerosol emission uncertainty as the global SSP scenarios (when other socioeconomic drivers are also accounted for). Capturing the full range of future aerosol uncertainty is particularly important, as it will enable us to further our understanding of potential future global and regional climate responses beyond the limits of the current RCP scenarios and illustrate what role air quality measures in industrialized and industrializing economies, alone, can play.

The following transient CLE and MTFR experiments add information beyond the idealized experiments presented so far, in that they explore the climate implications of potential plausible scenarios where users can reasonably be expected to understand and make their own near-term value judgements about the likelihood and impacts of these two scenarios. Further, this analysis will do the following:

- Illustrate the time scale over which these changes emerge.
- Illustrate how these changes could manifest themselves relative to natural variability in the climate system by comparing the climate change response across multiple ensemble members. This illustrates both the emergence of the climate signals (e.g., 20-yr mean changes) and also the likelihood of experiencing either dry or wet extreme years (which are also influenced by which scenario is followed).
- Provide an opportunity to assess the potential robustness of the results by comparing the responses in different models. Output from three climate model configurations is available (HadGEM3-GC2, GFDL CM3, and NorESM1-M).

1) Model setup

HadGEM3-GC2, the Hadley Centre model used to explore the climate response to these scenarios (Williams et al. 2015) differs from the configuration used in the earlier idealized experiments (HadGEM3-ES) as it uses atmospheric version HadGEM3-GA6 (compared to HadGEM3-GA4, used in HadGEM3-ES), which included an updated atmospheric dynamics scheme (Even Newer Dynamics for Global Atmospheric Modeling of the Environment). HadGEM3-GC2 also has a higher resolution (N216 vs N96 atmosphere, ¼° vs 1° ocean). It does share the same underlying aerosol parameterization (CLASSIC) as the version used in the earlier idealized experiments.

Results from two further CMIP5 generation models, GFDL CM3 (Griffies et al. 2011) and NorESM1-M (Iversen et al. 2013; Bentsen et al. 2013; Acosta Navarro et al. 2017) are also presented here. These provide an indication of the likely robustness of the projected changes given differences in the underlying model formulations. The HadGEM3-GC2 runs included four ensemble members initialized from 2005, NorESM1-M has three members from 2006, and GFDL CM3 has three members from 2005.

All three climate models are driven by two common ECLIPSE scenarios. These are both based on RCP4.5, so future greenhouse gas changes follow that pathway. The two scenarios differ in their aerosol emissions, with their either emissions following those under CLE air quality measures only or exploring what emissions would look like were MTFR to take place (Stohl et al. 2015). Here we compare future simulations between 2015 and 2050 for HadGEM3-GC2, GFDL CM3, and NorESM1-M. While aerosol emissions are changed globally, the largest differences in these two scenarios are located in Asia (Fig. 1).

The ECLIPSE simulations differ from the earlier idealized experiments in that they capture the time evolution of projected changes, sample emission pathways that can be linked back to real-world air quality decisions in industrialized economies, sample changes in a broader range of nonsulfate aerosols such as black carbon emissions, explore emissions that fall outside the Northern Hemispheric midlatitude region in the idealized runs, and in the case of HadGEM3-GC2 explore a higher-resolution climate model configuration. Where the climate response to differences between ECLIPSE scenarios resembles that seen in the idealized simulations, this may point to Northern Hemisphere midlatitude SO_2 emission cuts as being the important driver.

2) East and West African impacts

Figures 8 and 9 illustrate the East and West African precipitation response (respectively) to a reduction of global aerosols from CLE to MTFR. For this analysis, the contour panels of both figures looked at the average difference from 2030 to 2050. HadGEM3-GC2 (upper panel of Fig. 8) shows a similar response pattern to that illustrated in the idealized experiments. Similar features are also evident in GFDL CM3 (center, Fig. 8), with

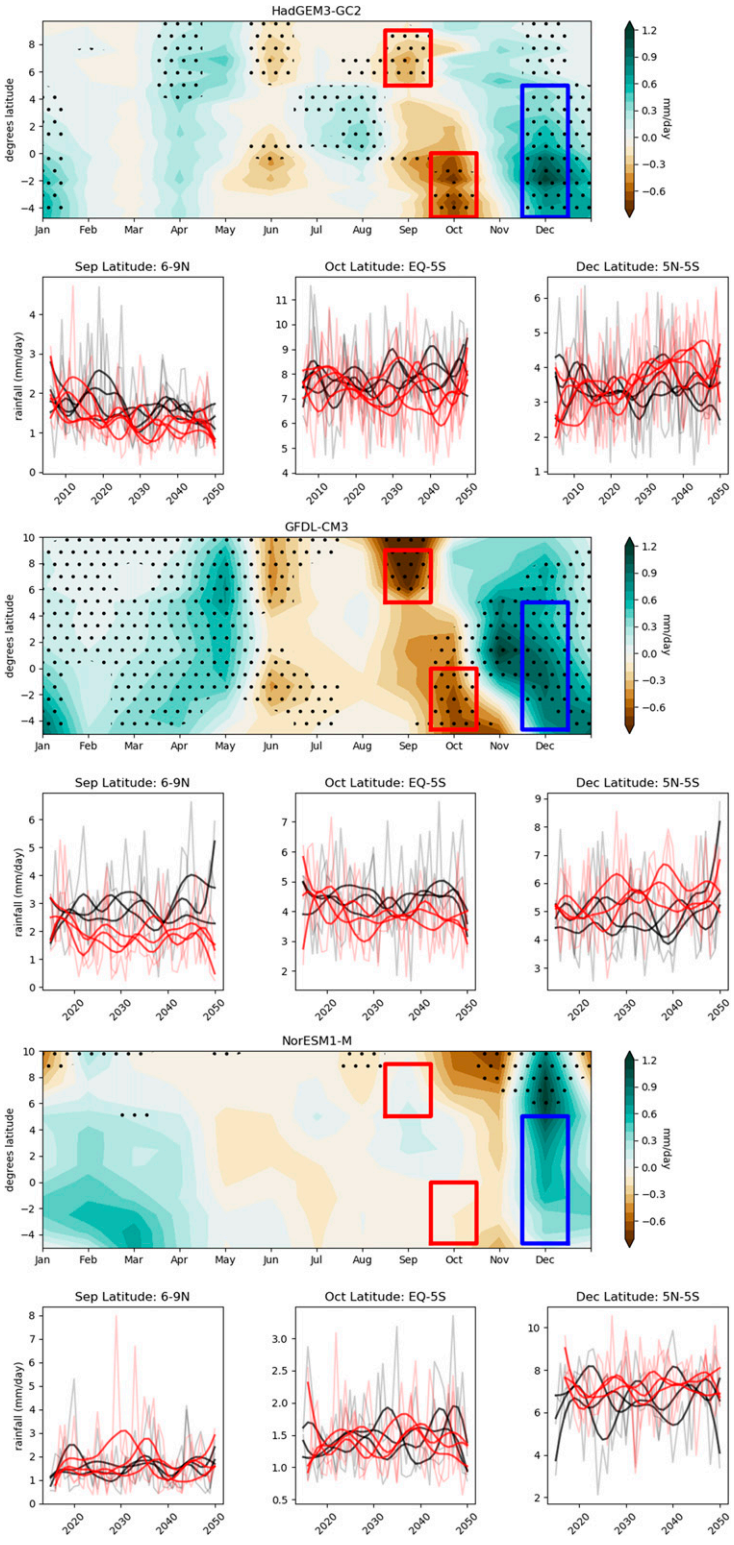

FIG. 8. Hovmöller maps of 2030–50 monthly average precipitation response difference (MTFR − CLE) over the East African domain for the (top) HadGEM3-GC2, (middle) GFDL CM3, and (bottom) NorESM1-M experiments. The Hovmöller plots show latitude (y axis) by season (x axis) changes for East Africa, averaging over all longitudes in the region shown in Fig. 2.

stronger significance, but the more northward displacement of the monsoon rainfall systems is evident across the whole annual cycle with wetter November to May conditions and a drier June–October period. A similar delay to the short rain onset and withdrawal (October–March) is also evident in NorESM1-M (bottom, Fig. 8) but the changes are not significant (except in north Somalia) and do not project on to the rest of the annual cycle.

The time evolution of the precipitation response for the three models is shown in Fig. 8 for three regions and months for which the 2030–50 mean difference between CLE and MTFR scenarios is significant in HadGEM3-GC2 at the 90% level, compared to 20-yr variability between ensemble members in the CLE experiment. These regions were chosen to illustrate the delayed onset (that occurs earlier in the north than the south) and later withdrawal of the short rains. This shows the time evolving nature, such as time of emergence (approximately 2025 for HadGEM-GC2 and earlier for GFDL CM3) when aerosol changes have an impact. Here all models point to an enhancement of precipitation in December only. Both HadGEM3-GC2 and GFDL CM3 agree and point to decreases in precipitation in September and October, matching the signal observed in the idealized experiments. The weaker response seen in NorESM1-M could in part be due to a weaker magnitude aerosol forcing compared to the other two models. Therefore, it may require a longer time period in order to see the aerosol response (Zelinka et al. 2014).

The individual ensemble members (faded lines in time series panels of Fig. 8) provide insight into the impact of these changes relative to the year-to-year and decade-to-decade variability in the region. Where the time series do diverge, they do so on the same time scales that the emissions diverge (Fig. 1). For both HadGEM3-GC2 and GFDL CM3, 11-yr running means of all MTFR members (smoothed red lines) become drier compared to CLE members (smoothed black lines) for September and October. Similarly, all three experiments show MTFR members to be wetter than CLE members for December. Where aerosol changes do drive differences, natural variability still leads to wet and dry years (see individual ensemble members). Taking December rainfall panels as an example, extreme dry years more frequently occur under a CLE scenario, while emission reductions under MTFR show greater frequency of wetter extremes. We see consensus for the December changes between all three models, but the enhanced drying in September and October (linked to the delayed onset) only cleanly emerges in HadGEM3-GC2 and GFDL CM3.

In West Africa, taking HadGEM3-GC2 simulations first (Fig. 9, left panel), MTFR sees rainfall increases along much, but not all, of the Sahel with reduced rainfall farther south. This is consistent with a northward shift of the rainbands. The main regions affected in the June to August rainfall increase, in terms of absolute magnitude changes, are in West Africa, along the Atlantic coastal region, including Sierra Leone, Liberia, and noncoastal Ivory Coast, and in the eastern Sahel region (encompassing southern Chad, northern Central African Republic, South Sudan, southern Sudan, and eastern Ethiopia). Both regions see an increase in the 20-yr climatological rainfall of roughly 1 mm day^{-1}; however, in the relatively drier central and eastern Sahel region this increase represents a much larger (20%) fractional increase on present-day rainfall levels. The changes in northward displacement of the tropical rainband are broadly similar to the pattern of change in the precipitation response to the idealized removal of Northern Hemispheric aerosols shown earlier in Fig. 7; however, they differ in their latitudinal location, and surprisingly they are larger in magnitude. In particular, the eastern Sahel region (from southern Chad to Ethiopia) shows enhanced rainfall increases compared to the idealized experiment. It is not clear whether these differences arise from the inclusion of aerosol reductions of South Asia and/or nonsulfate aerosol both included in these transient experiments (which were not accounted for in the idealized runs, Fig. 4) or are due to transient responses of the Atlantic to these changes (which would not be captured in the long multicentennial mean idealized responses). They could also

←

Statistical significance of these differences is indicated by dots. This significance is calculated at the 10% level relative to internal variability in 2030–50 mean rainfall across the CLE ensemble. Time series panels show monthly rainfall for September (north Somalia), October (south Kenya, Great Lakes and north Tanzania), and December (Kenya, Uganda, Great Lakes, and north Tanzania) for individual ensemble members. Red lines represent MTFR and black lines represent CLE. Prominent lines are 11-yr smoothed versions of the annual lines, using a Hanning filter; the emphasis changes on longer climatological time scales.

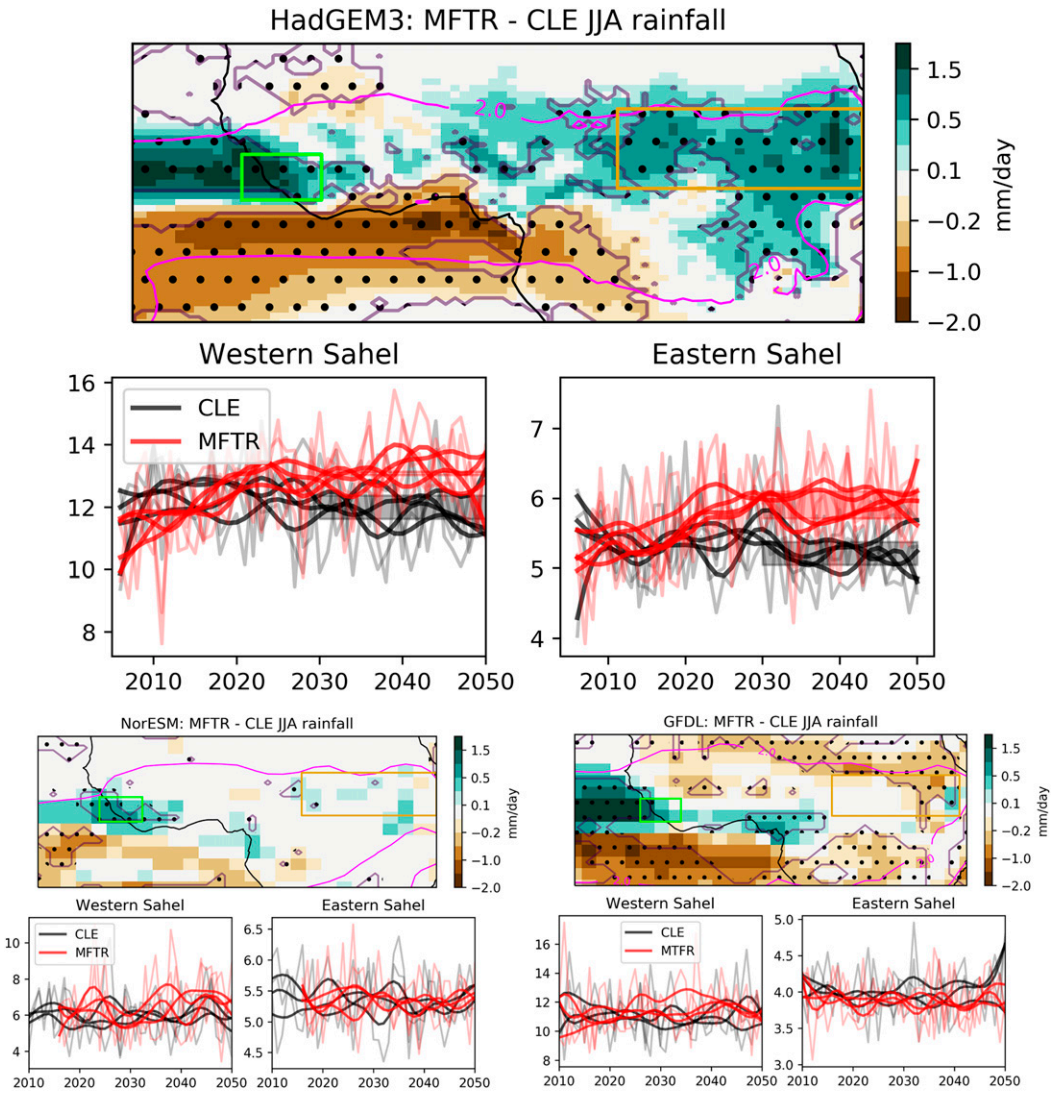

FIG. 9. CLE/MTFR scenarios: Rainfall in the maximum feasible reduction vs current legislation scenarios for three climate models. (top) The response from the HadGEM3-GC2 model while shown below are the responses from the (bottom left) NorESM1-M and (bottom right) GFDL CM3 models. The spatial response for 2030–50 mean rainfall changes is based on differences between the ensemble mean averages from the two scenarios. The dots indicate where these changes are significant at the 10% level, relative to the CLE ensemble 2030–50 spread. The time series panels show the changes for two regions (indicated by the boxes on the contour plots) for individual ensemble members, illustrating their annual variability (thin lines) and interannual variability (11-yr moving window, thick lines) for CLE (black) and MTFR (red). The spread of 2030–50 mean rainfall across each ensemble is indicated by the shaded bars for the HadGEM3-GC2 time series.

in part be a result of the resolution differences between the models (HadGEM-GC2 runs uses a 0.25° ocean resolution while the idealized experiments used 1°, and N216 vs N96 in the atmosphere) or differences in the dynamical core of the models [see section 3b(1)].

Comparing with the other two models (GFDL CM3 and NorESM1-M) points to a robustness of response patterns (but not magnitude) for a southern tropical rainband shift over the Atlantic coast (Fig. 9). However, projected changes over the interior of the Sahel are not robust across the models (Fig. 9). NorESM1-M captures very little change away from the coasts. In contrast, GFDL CM3 suggests a strong contraction of the Sahel rainfall (with reduced rainfall on both the northern and southern tails in central and eastern Sahel) rather than the southward migration that we see in the Atlantic.

GFDL CM3 simulates strong East Asian aerosol forcing, but it is not clear whether we should expect model differences in aerosol forcing in East Asia would explain a suppressed Sahel rainfall (Grandey et al. 2016) or not (Grandey et al. 2018). These results suggest a greater degree of consensus on the impact of aerosol changes in the western Sahel bordering the coast. While the aerosol emission scenarios do have a potential to substantially impact Sahel rainfall in central and eastern regions (wetting in HadGEM3-GC2 and drying in GFDL CM3), there appears to be no consensus in these regions.

The individual ensemble members (time series, Fig. 9) again provide insight into the impact of these changes relative to the year-to-year variability in the region. Taking the western region first, while this interannual variability is larger than the 20-yr climatological change, the climatological change is still substantial. Both the wet and dry years are roughly 1 mm day^{-1} (HadGEM3-GC2 and GFDL CM3) or 0.5 mm day^{-1} (NorESM1-M) wetter under the MTFR scenario. Unlike greenhouse gas scenarios, the Sahel rainfall responds quickly to the air quality changes, with the decadal rainfall clearly separating (smoothed time series in Fig. 9) as the emission differences (Fig. 1) increase to their 2030 maximum extent. The aerosol changes also have implications for the extremes, with all models projecting greater frequency of dry JJA seasons under CLE scenarios compared to the greater frequency wet seasons under MTFR scenarios. In the eastern region, the time series illustrate similar features. Where emission cuts (MTFR) lead to moistening (HadGEM3-GC2) or drying (GFDL CM3), these changes impact both the mean and likelihood of experiencing extreme dry or wet conditions and these impacts are felt on the same time scale that the emissions changes are occurring.

The rainfall impacts of these scenarios illustrate the potential vulnerability of East and West African rainfall to air quality policy in remote industrialized and industrializing economies. The impacts illustrated here would be expected to be strongly felt in the regions and seasons highlighted (boxed regions in figures). It is worth noting that the HadGEM3-GC2 and GFDL CM3 models have aerosol radiative forcings (a metric of the impact of aerosols on global climate) on the upper end of the current CMIP5 multimodel ranges. The changes in NorESM1-M are at the lower end of the range from CMIP5 models that represent indirect effects (Zelinka et al. 2014). Allen et al. (2015) suggest that the magnitude of aerosol forcing gradient across the equator is correlated with aerosol impact on simulated tropical rainfall shifts. So, if the real world exhibited smaller aerosol forcing, then a smaller rainfall impact (closer to that simulated by NorESM1-M) should be expected.

Large magnitude changes shown by the more sensitive models, however, should not necessarily be dismissed, particularly over West Africa. Allen et al. (2015) showed that the models that did better at capturing the historical southward 1950–80 rainfall shift were the models with the larger aerosol sensitivities and so there are reasons to consider these models when looking at future projections. HadGEM3-GC2 in particular has been shown to be one of the better models in capturing Sahel rainfall across the interior (Vellinga et al. 2016) and captures well the observed relationships between Sahel rainfall and SSTs on annual and multiannual time scales (Sheen et al. 2017). Similarly, Kasoar et al. (2016) showed that while this model had some of the strongest aerosol response over Asia it also was also one of the best at reproducing present-day aerosol metrics [such as aerosol optical depth (AOD)]. The impact of air quality on rainfall will also depend on the greenhouse gas pathways. These experiments explore air quality impacts around a single RCP pathway (RCP4.5 in this case).

This work highlights the need for climate simulations to explore this wider influence of both greenhouse gas pathways and air quality scenarios. CMIP6 will represent a step forward in this regard with a greater range of socioeconomic drivers of near-term aerosol emissions, but we cannot expect these new scenarios to span the full range as they are not designed to explicitly account for air quality drivers as the CLE and MTFR scenarios do here.

4. Discussion and conclusions

There is already an existing literature that links historical anthropogenic aerosol emission changes to past shifts in African rainfall via a shift in the tropical rainbands (Rotstayn and Lohmann 2002; Chang et al. 2011; Bollasina et al. 2011; Allen et al. 2015). Similarly, projected future aerosol declines have been shown to drive a northward shift in the tropical monsoon systems (Allen 2015; Rotstayn et al. 2015). Earlier idealized experiments linked removal of North American and European SO_2 emissions to moister conditions in the Sahel in two out of three climate models (Westervelt et al. 2017, 2018). Here we extend this analysis over West Africa by exploring for the first time the temporal evolution of rainfall changes under two scenarios designed to span much of the current uncertainty in future aerosol emission pathways, with climate projections from three climate models. We use similarities in the response with a parallel idealized experiment, where only SO_2 emissions are removed, to infer how important they may be in understand the range in rainfall responses. For East Africa, no existing studies have made links between future aerosol emission changes and

rainfall. However, factors that influence the mean position of the tropical monsoon systems may also be expected to project onto East African rainfall. Here we illustrate how important these impacts may be, using the same set of scenario and idealized experiments.

First, we use idealized model experiments (section 2) to explore what climate effect we would expect from a complete removal of industrial sulfates across the Northern Hemisphere midlatitude (NHML) region on East and West Africa. Sulfate aerosols are not the only aerosol pollutant, but changes in sulfates are thought to represent the dominant global aerosol driver of tropical rainfall shifts (Allen et al. 2015; Allen 2015). These idealized experiments confirm expectations from previous work (Westervelt et al. 2017, 2018), showing aerosol emission cuts preferentially warming the Northern Hemisphere, leading to a general northward shift of the tropical rain over the Sahel. These experiments do also suggest that aerosol emission changes can be expected to impact East African rainfall. These new findings suggest that any future emission cuts will result in a later onset of the short rains and a subsequent wetter season as the southward withdrawal is delayed. This delayed timing of the short rains is linked to an enhanced Arabian heat low in late boreal summer/autumn. In West Africa, these same enhanced north–south gradients lead to wetter Sahel conditions during the monsoon season (JJA), as the Saharan heat low builds through the season.

The wider set of potential emission scenarios [such as CMIP6's SSP scenarios (O'Neill et al. 2016; Riahi et al. 2017)] project a range of future aerosol emission changes between little at all [some fossil fuel (SSP5) scenarios with business as usual assumptions] to those that realize close to 90% emission cuts relative to present day (aggressive mitigation scenarios with strong decarbonization) over the next 30–40 years (Fig. 1). When informing African climate adaptation decisions over this near-term horizon, it is tempting to utilize climate projections from the multimodel archive. However, existing CMIP5-era climate projections all share similar aerosol emission pathways and do not sample the wider near-term (10–40 yr) aerosol scenario range in Fig. 1. As we, and others (e.g., Westervelt et al. 2018), have shown that we can expect these wider potential aerosol pathways to drive African rainfall change, then this suggests caution in any over reliance on CMIP5 projections, alone, to inform these decisions. If the world experiences more rapid reductions than CMIP5 projections, we would expect to see larger impacts (wetter Sahel, larger delays in East African short rain onset and withdrawal) than those projected within CMIP5. However, should the real-world emissions show little reduction, then we would expect very little of these aerosol linked changes (i.e., drier conditions in coastal western Sahel, drier rainfall conditions in East African December and January, and little impact on short rains onset). As projections based on current CMIP5 generation models include aerosol emission cuts that do not explore this wider emission uncertainty and that lie between these two edge cases, this context necessitates caution in interpreting climate projections from existing climate models over West or East Africa. To take the delayed short rains onset (and subsequent rainfall enhancement) due to aerosol emission reductions as an example, Dunning et al. (2018) identified a similar response in CMIP5 RCP climate projections. If, as speculated here, the CMIP5 model response arises due to reductions in aerosol emissions, then should the real world follow a pathway with no cuts beyond current legislated air quality measures on one hand compared to a scenario with more aggressive air quality cuts on the other, then this signal would either be expected to be absent or enhanced (respectively). If these rainfall signals are indeed deemed the dominant drivers of near-term East and West African rainfall uncertainty, then our work motivates the need for a greater emphasis and experiments that explore near-term aerosol emission scenarios rather than just end of century GHG pathways.

In section 3 we explored explicit air quality scenario simulations from HadGEM3-GC2, GDFL CM3, and NorESM1-M that provide insight into the time scale that aerosol scenario driven changes can be expected to manifest; the importance of these changes relative to internal variability; and how robust these changes are given uncertainties in representation of climate model processes. The multimodel comparison points toward a general model agreement on the northward shift of the tropical rainbands, but the local impacts are not always robust. In East Africa, models agree on the enhanced precipitation in December and January due to the delayed southward withdrawal of the seasonal rainfall; however, models do not show consensus on the delayed onset (captured by HadGEM3-GC2 and GFDL CM3, but not NorESM1-M; Fig. 8). For West Africa, the models agree on the pattern, if not the magnitude of rainfall impacts along the Atlantic coasts but show little consensus in the Sahel interior. The potential demonstrated for stronger moistening (HadGEM3-GC2) or drying (GFDL CM3) due to aerosol scenarios with larger emission cuts, motivates the urgent need for further work to understand the sources of these model differences.

Some care is needed in interpreting uncertainties in the African rainfall projections. Climate models have been shown to struggle in reproducing present day the West African monsoon, with common southward biases in the monsoon position (e.g., Martin et al. 2014) and

often inadequate teleconnections between Sahel rainfall and ocean temperature changes (Rowell 2013; Martin et al. 2014). While some models do better at these processes, deficiencies in many models in reproducing the rainfall response has been linked to weakly captured or missing feedback mechanisms—particularly, wind–evaporation–sea surface temperature (WES) feedbacks, low cloud feedbacks, and either missing or inadequately coupled dust feedbacks (Wang et al. 2012; Martin et al. 2014; Rowell 2019). These feedbacks will all tend to enhance any cross-equatorial temperature gradient, leading to larger magnitude monsoon shifts, and weaknesses in capturing these process means that many models underestimate Sahel rainfall responses. Model differences in aerosol forcing gradients across the equator have also been linked to whether a model can capture the magnitude of historical Sahel rainfall responses, with larger forcing gradients better able to reproduce historical shifts (Allen et al. 2015). HadGEM3-GC2 has been shown to be one of the better models, historically (Vellinga et al. 2016; Sheen et al. 2017), but with only three models we lack the information to assess which of the presented projections are more likely, and we also caution that standard metrics of past performance are not necessarily a reliable guide to projection performance (e.g., Rowell et al. 2016). By highlighting that aerosol emission scenarios have a potential to drive large shifts in African rainfall in the near-term 10–40-yr horizon, our work motivates the need for larger climate model ensemble approaches to inform on the projected impacts.

Despite some lack of model consensus for particular components of the aerosol–precipitation signal, these results still offer a unique perspective into future rainfall changes in Africa. They illustrate how strongly these impacts could be felt within the context of interdecadal variability. The time series in both East and West Africa diverge on a similar time scale (time series, Figs. 8 and 9) to the divergence of the emission pathways (Fig. 1). The divergence due to aerosol/air quality pathways would be apparent in a number of key regions (25% wetter under MFTR scenario in the eastern Sahel, for example). They will also be expected to have an impact on extremes. In coastal West Africa for example, while individual years can still be expected to show changes larger than the 20-yr climatological differences, there is a clear indication that extreme dry years are more likely to occur under current legislation (CLE) scenarios than a maximum technological feasible reduction (MTFR) scenario. Likewise, extreme wet conditions are more likely to occur under the MTFR scenario.

The rapid emergence of the climate signal in response to emission cuts poses interesting questions about how we inform climate adaptation in Africa. This rapid emergence is in contrast to the climate response to GHGs, where very long atmospheric lifetimes (roughly 80-yr time scales for CO_2) lead to a much slower climate adjustment to GHG emission changes (Hawkins and Sutton 2009). This highlights the importance of translating the current level of international commitment to reducing air pollutants into 5–10-yr climate outlooks. The ECLIPSE scenarios are a good example of this. The CLE scenario, for example, illustrates how current commitments can be translated to emission pathways, and then through modeling to climate impacts. Revised estimates of emission impacts of legislated measures every 5–10 years would have a value in providing near-term climate adaptation information for African stakeholders.

This work highlights previously unexplored vulnerability of future East African rainfall to remote air quality pathways and provides further support for currently known West African aerosol–precipitation vulnerabilities, with new scenarios that envelop potential 10–40-yr air quality pathways. It motivates the need for new emission scenarios (or adoption of existing scenarios like ECLIPSE) and a wider number of global climate model simulations. These are needed both to assess the wider robustness of these projected changes and to provide the evidence to underpin climate adaptation in these regions, most vulnerable to future shifts in near-term climate. It highlights the value of revisiting and updating these scenarios as current commitments evolve. Doing so, however, will require commitment from both the integrated assessment modeling that underpins the emission scenarios and climate modeling groups that translate these to climate impacts. Our work highlighting the potential impacts, illustrates the importance that such future work would have.

Acknowledgments. This work was funded by the U.K. Department for International Development (DFID)/Natural Environment Research Council (NERC) Future Climate for Africa (FCFA) HyCRISTAL project Grant NE/M019985/1 and the NERC/DFID Future Climate for Africa programme under the AMMA-2050 project, Grant NE/M019977/1. LJW was supported by the U.K.-China Research and Innovation Partnership Fund through the Met Office Climate Science for Service Partnership (CSSP) China as part of the Newton Fund. MK and AV would like to thank the Natural Environment Research Council for funding. Simulations with HadGEM3-GA4/HadGEM3-GC1 were performed using the MONSooN system, a collaborative facility supplied under the Joint Weather and Climate Research Programme, which is a strategic partnership between the Met Office and the Natural Environment

Research Council. JCAN was supported by the personal Grant Juan de la Cierva FJCI-2017-34027 from the Spanish Ministerio de Economía y Competitividad (MINECO). The NorESM work was supported by the Research Council of Norway through the EarthClim (207711/E10) and NOTUR/NorStore projects (nn2345k/ns2345k) and through the European Commission FP7 project PEGASOS (FP7-ENV-2010-265148). We thank Vaishali Naik for her review and processing of the ECLIPSE emissions for the GFDL CM3 runs.

REFERENCES

Ackerley, D., B. B. Booth, S. H. Knight, E. J. Highwood, D. J. Frame, M. R. Allen, and D.P. Rowell, 2011: Sensitivity of twentieth-century Sahel rainfall to sulfate aerosol and CO_2 forcing. *J. Climate*, **24**, 4999–5014, https://doi.org/10.1175/JCLI-D-11-00019.1.

Acosta Navarro, J. C., and Coauthors, 2017: Future response of temperature and precipitation to reduced aerosol emissions as compared with increased greenhouse gas concentrations. *J. Climate*, **30**, 939–954, https://doi.org/10.1175/JCLI-D-16-0466.1.

Allen, R. J., 2015: A 21st century northward tropical precipitation shift caused by future anthropogenic aerosol reductions. *J. Geophys. Res. Atmos.*, **120**, 9087–9102, https://doi.org/10.1002/2015JD023623.

——, A. T. Evan, and B. B. B. Booth, 2015: Interhemispheric aerosol radiative forcing and tropical precipitation shifts during the late twentieth century. *J. Climate*, **28**, 8219–8246, https://doi.org/10.1175/JCLI-D-15-0148.1.

Amann, M., Z. Klimon, and F. Wagner, 2013: Regional and global emissions of air pollutants: Recent trends and future scenarios. *Annu. Rev. Environ. Resour.*, **38**, 31–35, https://doi.org/10.1146/annurev-environ-052912-173303.

Bellouin, N., J. Rae, A. Jones, C. Johnson, J. Haywood, and O. Boucher, 2011: Aerosol forcing in the Climate Model Intercomparison Project (CMIP5) simulations by HadGEM2-ES and the role of ammonium nitrate. *J. Geophys. Res.*, **116**, D20206, https://doi.org/10.1029/2011JD016074.

Bentsen, M., and Coauthors, 2013: The Norwegian Earth System Model, NorESM1-M—Part 1: Description and basic evaluation of the physical climate. *Geosci. Model Dev.*, **6**, 687–720, https://doi.org/10.5194/gmd-6-687-2013.

Bollasina, M. A., Y. Ming, and V. Ramaswamy, 2011: Anthropogenic aerosols and the weakening of the South Asian summer monsoon. *Science*, **334**, 502–505, https://doi.org/10.1126/science.1204994.

Booth, B. B. B., N. J. Dunstone, P. R Halloran, T. Andrews, and N. Bellouin, 2012: Aerosols implicated as a prime driver of twentieth-century North Atlantic climate variability. *Nature*, **484**, 228–232, https://doi.org/10.1038/NATURE10946.

Chadwick, R., 2016: Which aspects of CO_2 forcing and SST warming cause most uncertainty in projections of tropical rainfall change over land and ocean? *J. Climate*, **29**, 2493–2509, https://doi.org/10.1175/JCLI-D-15-0777.1.

Chang, C., J. C. Chiang, M. F. Wehner, A. R. Friedman, and R. Ruedy, 2011: Sulfate aerosol control of tropical Atlantic climate over the twentieth century. *J. Climate*, **24**, 2540–2555, https://doi.org/10.1175/2010JCLI4065.1.

Dai, A., 2012: Increasing drought under global warming in observations and models. *Nat. Climate Change*, **3**, 52–58, https://doi.org/10.1038/NCLIMATE1633.

——, P. J. Lamb, K. E. Trenberth, M. Hulme, P. D. Jones, and P. P. Xie, 2004: The recent Sahel drought is real. *Int. J. Climatol.*, **24**, 1323–1331, https://doi.org/10.1002/joc.1083.

Dong, B., and R. Sutton, 2015: Dominant role of greenhouse-gas forcing in the recovery of Sahel rainfall. *Nat. Climate Change*, **5**, 757–760, https://doi.org/10.1038/nclimate2664.

——, ——, E. Highwood, and L. Wilcox, 2014: The impacts of European and Asian anthropogenic sulfur dioxide emissions on Sahel rainfall. *J. Climate*, **27**, 7000–7017, https://doi.org/10.1175/JCLI-D-13-00769.1.

Dunning, C. M., E. Black, and R. P. Allan, 2018: Later wet seasons with more intense rainfall over Africa under future climate change. *J. Climate*, **31**, 9719–9738, https://doi.org/10.1175/JCLI-D-18-0102.1.

Grandey, B. S., H. Cheng, and C. Wang, 2016: Transient climate impacts for scenarios of aerosol emissions from Asia: A story of coal versus gas. *J. Climate*, **29**, 2849–2867, https://doi.org/10.1175/JCLI-D-15-0555.1.

——, L. K. Yeo, H. H. Lee, and C. Wang, 2018: The equilibrium climate response to sulfur dioxide and carbonaceous aerosol emissions from East and Southeast Asia. *Geophys. Res. Lett.*, **45**, 11 318–11 325, https://doi.org/10.1029/2018GL080127.

Griffies, S. M., and Coauthors, 2011: The GFDL CM3 coupled climate model: Characteristics of the ocean and sea ice simulations. *J. Climate*, **24**, 3520–3544, https://doi.org/10.1175/2011JCLI3964.1.

Hardiman, S. C., N. Butchart, F. M. O'Connor, and S. T. Rumbold, 2017: The Met Office HadGEM3-ES chemistry–climate model: Evaluation of stratospheric dynamics and its impact on ozone. *Geosci. Model Dev.*, **10**, 1209–1232, https://doi.org/10.5194/gmd-10-1209-2017.

Hawkins, E., and R. Sutton, 2009: The potential to narrow uncertainty in regional climate predictions. *Bull. Amer. Meteor. Soc.*, **99**, 1095–1108, https://doi.org/10.1175/2009BAMS2607.1.

Held, I. M., T. L. Delworth, J. Lu, K. L. Findell, and T. R. Knutson, 2005: Simulation of Sahel drought in the 20th and 21st centuries. *Proc. Natl. Acad. Sci. USA*, **102**, 17 891–17 896, https://doi.org/10.1073/pnas.0509057102.

Hoerling, M., J. Hurrell, J. Eischeid, and A. Phillips, 2006: Detection and attribution of twentieth-century northern and southern African rainfall change. *J. Climate*, **19**, 3989–4008, https://doi.org/10.1175/JCLI3842.1.

Hwang, Y.-T., D. M. W. Frierson, and S. M. Kang, 2013: Anthropogenic sulfate aerosol and the southward shift of tropical precipitation in the late 20th century. *Geophys. Res. Lett.*, **40**, 2845–2850, https://doi.org/10.1002/GRL.50502.

IPCC, 2014a: *Climate Change 2014: Impacts, Adaptation, and Vulnerability. Part A: Global and Sectoral Aspects*. C. B. Field et al., Eds., Cambridge University Press, 1132 pp., http://www.ipcc.ch/pdf/assessment-report/ar5/wg2/WGIIAR5-PartA_FINAL.pdf.

——, 2014b: *Climate Change 2014: Impacts, Adaptation, and Vulnerability. Part B: Regional Aspects*. V. R. Barros et al., Eds., Cambridge University Press, 688 pp., http://www.ipcc.ch/pdf/assessment-report/ar5/wg2/WGIIAR5-PartB_FINAL.pdf.

Iversen, T., and Coauthors, 2013: The Norwegian Earth System Model, NorESM1-M—Part 2: Climate response and scenario

projections. *Geosci. Model Dev.*, **6**, 389–415, https://doi.org/10.5194/gmd-6-389-2013.

Kasoar, M., A. Voulgarakis, J.-F. Lamarque, D. T. Shindell, N. Bellouin, W. J. Collins, G. Faluvegi, and K. Tsigaridis, 2016: Regional and global temperature response to anthropogenic SO_2 emissions from China in three climate models. *Atmos. Chem. Phys.*, **16**, 9785–9804, https://doi.org/10.5194/ACP-16-9785-2016.

——, D. Shawki, and A. Voulgarakis, 2018: Similar spatial patterns of global climate response to aerosols from different regions. *npj Climate Atmos. Sci.*, **1**, 12, https://doi.org/10.1038/S41612-018-0022-Z.

Kawase, H., M. Abe, Y. Yamada, T. Takemura, T. Yokohata, and T. Nozawa, 2010: Physical mechanism of long-term drying trend over tropical North Africa. *Geophys. Res. Lett.*, **37**, L09706, https://doi.org/10.1029/2010GL043038.

Liebmann, B., and Coauthors, 2014: Understanding recent eastern Horn of Africa rainfall variability and change. *J. Climate*, **27**, 8630–8645, https://doi.org/10.1175/JCLI-D-13-00714.1.

Lu, Z., Q. Zhang, and D. G. Streets, 2011: Sulfur dioxide and primary carbonaceous aerosol emissions in China and India, 1996–2010. *Atmos. Chem. Phys.*, **11**, 9839–9864, https://doi.org/10.5194/acp-11-9839-2011.

Manktelow, P. T., G. W. Mann, K. S. Carslaw, D. V. Spracklen, and M. P. Chipperfield, 2007: Regional and global trends in sulfate aerosol since the 1980s. *Geophys. Res. Lett.*, **34**, L14803, https://doi.org/10.1029/2006GL028668.

Martin, E. R., C. Thorncroft, and B. B. Booth, 2014: The multidecadal Atlantic SST—Sahel rainfall teleconnection in CMIP5 simulations. *J. Climate*, **27**, 784–806, https://doi.org/10.1175/JCLI-D-13-00242.1.

Martin, G. M., M. A. Ringer, V. D. Pope, A. Jones, C. Dearden, and T. J. Hinton, 2006: The physical properties of the atmosphere in the new Hadley Centre Global Environmental Model (HadGEM1). Part I: Model description and global climatology. *J. Climate*, **19**, 1274–1301, https://doi.org/10.1175/JCLI3636.1.

——, and Coauthors, 2011: The HadGEM2 family of Met Office Unified Model climate configurations. *Geosci. Model Dev.*, **4**, 723–757, https://doi.org/10.5194/GMD-4-723-2011.

Myhre, G., and Coauthors, 2013: Anthropogenic and natural radiative forcing. *Climate Change 2013: The Physical Science Basis*, T. F. Stocker et al., Eds., Cambridge University Press, 659–740.

Nicholson, S. E., 2015: Long-term variability of the East African 'short rains' and its links to large-scale factors. *Int. J. Climatol.*, **35**, 3979–3990, https://doi.org/10.1002/joc.4259.

——, 2016: An analysis of recent rainfall conditions in eastern Africa. *Int. J. Climatol.*, **36**, 526–532, https://doi.org/10.1002/joc.4358.

——, 2017: Climate and climatic variability of rainfall over eastern Africa. *Rev. Geophys.*, **55**, 590–635, https://doi.org/10.1002/2016RG000544.

O'Neill, B. C., and Coauthors, 2016: The Scenario Model Intercomparison Project (ScenarioMIP) for CMIP6. *Geosci. Model Dev.*, **9**, 3461–3482, https://doi.org/10.5194/gmd-9-3461-2016.

Riahi, K., and Coauthors, 2017: The shared socioeconomic pathways and their energy, land use, and greenhouse gas emissions implications: An overview. *Global Environ. Change*, **42**, 153–168, https://doi.org/10.1016/j.gloenvcha.2016.05.009.

Rotstayn, L. D., and U. Lohmann, 2002: Tropical rainfall trends and the indirect aerosol effect. *J. Climate*, **15**, 2103–2116, https://doi.org/10.1175/1520-0442(2002)015<2103:TRTATI>2.0.CO;2.

——, M. A. Collier, and J. J. Luo, 2015: Effects of declining aerosols on projections of zonally averaged tropical precipitation. *Environ. Res. Lett.*, **10**, 044018, https://doi.org/10.1088/1748-9326/10/4/044018.

Rowell, D. P., 2013: Simulating SST teleconnections to Africa: What is the state of the art? *J. Climate*, **26**, 5397–5418, https://doi.org/10.1175/JCLI-D-12-00761.1.

——, 2019: An observational constraint on CMIP5 projections of the East African long rains and southern Indian Ocean warming. *Geophys. Res. Lett.*, **46**, 6050–6058, https://doi.org/10.1029/2019GL082847.

——, B. B. B. Booth, S. E. Nicholson, and P. Good, 2015: Reconciling past and future rainfall trends over East Africa. *J. Climate*, **28**, 9768–9788, https://doi.org/10.1175/JCLI-D-15-0140.1.

——, C. A. Senior, M. Vellinga, and R. J. Graham, 2016: Can climate projection uncertainty be constrained over Africa using metrics of contemporary performance? *Climatic Change*, **134**, 621–633, https://doi.org/10.1007/s10584-015-1554-4.

Shawki, D., A. Voulgarakis, A. Chakraborty, M. Kasoar, and J. Srinivasan, 2018: The South Asian Monsoon response to remote aerosols: Global and regional mechanisms. *J. Geophys. Res. Atmos.*, **123**, 11 585–11 601, https://doi.org/10.1029/2018JD028623.

Sheen, K. L, D. M. Smith, N. J. Dunstone, R. Eade, D. P. Rowell, and M. Vellinga, 2017: Skilful prediction of Sahel summer rainfall on inter-annual and multi-year timescales. *Nat. Commun.*, **8**, 14966, https://doi.org/10.1038/NCOMMS14966.

Shindell, D. T., A. Voulgarakis, G. Faluvegi, and G. Milly, 2012: Precipitation response to regional radiative forcing. *Atmos. Chem. Phys.*, **12**, 6969–6982, https://doi.org/10.5194/acp-12-6969-2012.

Stohl, A., and Coauthors, 2015: Evaluating the climate and air quality impacts of short-lived pollutants. *Atmos. Chem. Phys.*, **15**, 10 529–10 566, https://doi.org/10.5194/acp-15-10529-2015.

Undorf, S., M. A. Bollasina, and G. C. Hegerl, 2018: Impacts of the 1900–74 increase in anthropogenic aerosol emissions from North America and Europe on Eurasian summer climate. *J. Climate*, **31**, 8381–8399, https://doi.org/10.1175/JCLI-D-17-0850.1.

Van Vuuren, D. P., and Coauthors, 2011: The representative concentration pathways: An overview. *Climatic Change*, **109**, 5–31, https://doi.org/10.1007/S10584-011-0148-Z.

Vellinga, M., M. Roberts, P. L. Vidale, M. S. Mizielinski, M.-E. Demory, R. Schiemann, J. Strachan, and C. Bain, 2016: Sahel decadal rainfall variability and the role of model horizontal resolution. *Geophys. Res. Lett.*, **43**, 326–333, https://doi.org/10.1002/2015GL066690.

Viste, E., D. Korecha, and A. Sorteberg, 2013: Recent drought and precipitation tendencies in Ethiopia. *Theor. Appl. Climatol.*, **112**, 535–551, https://doi.org/10.1007/S00704-012-0746-3.

Walters, D. N., and Coauthors, 2014: The Met Office Unified Model Global Atmosphere 4.0 and JULES Global Land 4.0 configurations. *Geosci. Model Dev.*, **7**, 361–386, https://doi.org/10.5194/GMD-7-361-2014.

Wang, C., S. Dong, A. T. Evan, G. R. Foltz, and S. K. Lee, 2012: Multidecadal covariability of North Atlantic sea surface temperature, African dust, Sahel rainfall, and Atlantic hurricanes. *J. Climate*, **25**, 5404–5415, https://doi.org/10.1175/JCLI-D-11-00413.1.

Westervelt, D. M., and Coauthors, 2017: Multimodel precipitation responses to removal of U.S. sulfur dioxide emissions. *J. Geophys. Res. Atmos.*, **122**, 5024–5038, https://doi.org/10.1002/2017JD026756.

——, and Coauthors, 2018: Connecting regional aerosol emissions reductions to local and remote precipitation responses. *Atmos. Chem. Phys.*, **18**, 12 461–12 475, https://doi.org/10.5194/acp-18-12461-2018.

Wilcox, L. J., E. J. Highwood, and N. J. Dunstone, 2013: The influence of anthropogenic aerosol on multi-decadal variations of historical global climate. *Environ. Res. Lett.*, **8**, 024033, https://doi.org/10.1088/1748-9326/8/2/024033.

Williams, K. D., and Coauthors, 2015: The Met Office global coupled model 2.0 (GC2) configuration. *Geosci. Model Dev.*, **8**, 1509–1524, https://doi.org/10.5194/gmd-8-1509-2015.

Yang, W., R. Seager, M. A. Cane, and B. Lyon, 2015: The rainfall annual cycle bias over East Africa in CMIP5 coupled climate models. *J. Climate*, **28**, 9789–9802, https://doi.org/10.1175/JCLI-D-15-0323.1.

Zelinka, M. D., T. Andrews, P. M. Forster, and K. E. Taylor, 2014: Quantifying components of aerosol-cloud-radiation interactions in climate models. *J. Geophys. Res. Atmos.*, **119**, 7599–7615, https://doi.org/10.1002/2014JD021710.

Zheng, B., and Coauthors, 2018: Trends in China's anthropogenic emissions since 2010 as the consequence of clean air actions. *Atmos. Chem. Phys.*, **18**, 14 095–14 111, https://doi.org/10.5194/ACP-2018-374.